Poroelasticity of the Callovo–Oxfordian Claystone

Malik Belmokhtar, Pierre Delage, Siavash Ghabezloo, Anh Minh A.M. Tang, Hamza Menaceur, Nathalie Conil

▶ **To cite this version:**

Malik Belmokhtar, Pierre Delage, Siavash Ghabezloo, Anh Minh A.M. Tang, Hamza Menaceur, et al.. Poroelasticity of the Callovo–Oxfordian Claystone. Rock Mechanics and Rock Engineering, 2017, 50 (4), pp.871 - 889. 10.1007/s00603-016-1137-3 . hal-01515962

HAL Id: hal-01515962
https://enpc.hal.science/hal-01515962

Submitted on 28 Apr 2017

HAL is a multi-disciplinary open access archive for the deposit and dissemination of scientific research documents, whether they are published or not. The documents may come from teaching and research institutions in France or abroad, or from public or private research centers.

L'archive ouverte pluridisciplinaire **HAL**, est destinée au dépôt et à la diffusion de documents scientifiques de niveau recherche, publiés ou non, émanant des établissements d'enseignement et de recherche français ou étrangers, des laboratoires publics ou privés.

Manuscript Click here to download Manuscript Text-figure_captions-table_caption.docx

Poroelasticity of the Callovo-Oxfordian claystone

Malik Belmokhtar[1], Pierre Delage[1], Siavash Ghabezloo[1], Anh-Minh Tang[1], Hamza Menaceur[1,3], Nathalie Conil[2]

[1] Ecole des Ponts ParisTech, Laboratoire Navier/CERMES, 6-8 av. B. Pascal, F77455 Marne la Vallée, France
[2]Andra, Bure, France
[3]Now at LEMTA, Université de Lorraine, Nancy, France

Corresponding author : Malik Belmokhtar
E-mail : malik.belmokhtar@enpc.fr
Phone : 00 33 (0)1 64 15 35 39

Abstract

This work is devoted to an experimental investigation of the poroelastic behaviour of the Callovo-Oxfordian (COx) claystone, a potential host rock for the deep underground repository of high-level radioactive waste in France. Drained, undrained, pore pressure loading and unjacketed tests were carried out in a specially designed isotropic compression cell to determine the poroelastic parameters of fully saturated specimens. Great care was devoted to the saturation procedure and very small loading rates were used to ensure full drainage conditions in drained and pore pressure tests (0.5 kPa/min) and in the unjacketed test (2 kPa/min). High precision strain measurements were performed by ensuring direct contact between the LVDTs' stems and the specimen, allowing to stay within the elastic domain during the tests. A set of poroelastic parameters was determined on two specimens under different confining stresses and a very good compatibility between the data of different tests was found, giving confidence in the data obtained. The unjacketed test provided a directly reliable measurement of the unjacketed modulus (K_s = 21.73 GPa) that was afterwards confirmed by an indirect evaluation that shows the non-dependency of K_s with respect to the stress level. A stress dependent Biot's coefficient b was found equal to 0.87 and 0.91 under 10 MPa and 8 MPa of Terzaghi effective stress respectively. An analysis in the framework of transverse isotropic poroelasticity provided the anisotropic Biot effective stress coefficients b_1 (perpendicular to bedding) and b_2 (parallel to bedding) with a higher value in the direction parallel to bedding. These parameters are that of specimens cored and trimmed in the laboratory. Given the high sensitivity of the claystone to damage, the values obtained here, which could be overestimated by damage, are to be compared with values that could be get from in-situ testing.

Keywords: Claystone, poroelasticity, Biot's coefficient, unjacketed modulus, isotropic compression cell.

1. Introduction

A possible host rock for geological radioactive waste disposal in France is the Callovo-Oxfordian (COx) claystone, a sedimentary clayey rock from the Paris basin deposited 155 million years ago into a 150 m thick layer over a layer of Dogger limestone and covered by a layer of Oxfordian limestone. Detailed investigations on the properties of the COx claystone are carried out in the Underground Research Laboratory (URL) managed by Andra, the French agency for the management of radioactive waste, close to the village of Bure in Eastern France. The URL is located at a depth of 490 m, at which the clay fraction in the claystone is maximum and close to 50%. A detailed investigation of the in-situ state of stress in the Bure URL was conducted by Wileveau *et al*. (2007), providing the following stress values: vertical total stress σ_V = 12.7 MPa (lithostatic), major horizontal stress σ_H = 12.7-14.8 MPa, minor horizontal stress σ_h = 12.4 MPa and pore pressure u = 4.9 MPa. Typical characteristics of the COx claystone are a very low permeability (in order of 10^{-20} m^2) (Escoffier, 2002; Davy *et al*., 2007; Zhang, 2011 ; Menaceur *et al*., 2015a, 2015b), a high sorption capacity for radionuclides and a low diffusion coefficient resulting in very slow solute transfer.

To optimize the design of the galleries and disposal cells of a possible geological waste repository in the COx claystone, various investigations have been carried out to explore its hydromechanical behaviour (Chiarelli, 2000; Chiarelli *et al*., 2003; Zhang & Rothfuchs, 2004; Hoxha *et al*., 2007; Hu *et al*., 2013; Menaceur *et al*., 2015a, 2015b). As quoted by Menaceur *et al*. (2015b), the variability observed in published data can be linked to the different experimental procedures adopted by the different research groups involved, with respect to the state of saturation of the specimens and to the drainage conditions imposed during triaxial testing. The significant sensitivity of claystones to changes in water content has been observed by Zhang *et al*. (2012), Pham *et al*. (2007), Valès *et al*. (2004), Zhang and Rothfuchs (2004) and Chiarelli *et al*. (2003), with larger strength at lower degrees of saturation. The importance of adopting short drainage length to ensure good saturation (under stress conditions close to the in-situ ones) within a reasonable period of time (no longer than one week) has been demonstrated by Monfared *et al*. (2011a). Actually, short drainage length ensured satisfactory drainage conditions with homogeneous pore pressure field within the specimens, allowing to investigate the intrinsic response of low porosity specimens through fully drained tests with no excess pore pressure. In this regard, Monfared *et al*. (2011a) developed a new hollow cylinder triaxial apparatus with a drainage length of 10 mm. Hu *et al*. (2014) also tested small sized triaxial specimens (20 mm in diameter and 40 mm in height). The failure criteria obtained on COx specimens by Hu *et al*. (2013)

on fully saturated and fully drained specimens appeared to be compatible with that obtained on the hollow cylinder apparatus by Menaceur *et al*., (2015b) on specimens of comparable porosity. Imperfect saturation and drainage conditions are known to over-estimate the mechanical characteristics (larger stiffness and larger failure stress).

Rather few studies addressed the poroelastic response of claystones (Vincké *et al*., 1998; Escoffier, 2002; Bemer *et al*., 2004; Noiret *et al*., 2010). Existing data show that various values of the modulus of the solid phase K_s have been found, resulting in a large range of possible values of the Biot coefficient b, between 0.33 and 0.95 (Escoffier, 2002). This variability is due to several reasons: natural variability of the samples (mineralogy, water content, porosity...), coring and trimming procedures, testing protocols adopted with respect to saturation and drainage procedures… Currently, the b reference value adopted by Andra in numerical calculations is most often taken equal to 0.6 (Gens *et al*., 2007; Charlier *et al*., 2013). However, because of these incertitude, it seems hence necessary to further investigate the poro-elastic behaviour of the COx claystone so as to provide more reliable values of the poro-elastic parameters and to reduce their variability for poro-elastic calculations. To do so, a special isotropic compression cell developed by Tang *et al*. (2008) and adapted by Mohajerani *et al*. (2012) was used and further developed in this work. In this device, a reduced drainage length (10 mm) is ensured by using a 10 mm thick specimen drained at bottom. A high precision local strains measurements device was developed to allow a precise determination of the poro-elastic parameters of the Callovo-Oxfordian claystone that were investigated along various hydromechanical paths.

2. Poroelastic framework

The Callovo-Oxfordian claystone is a saturated porous medium in which the solid phase is made up of various components that will be described in more details later on. This section successively recalls the fundamentals of poroelasticity of fully saturated porous media, first in isotropic conditions and then in the case of transverse isotropy, a case more adapted to sedimentary soils and rocks. The investigation carried out here is based on the use of an isotropic compression cell providing a hydrostatic stress state.

The changes in volumetric strain ε_v ($\varepsilon_v = \varepsilon_1 + \varepsilon_2$) in which ε_1 and ε_2 are the strains along the axial direction 1 and the radial direction 2, respectively with respect to changes in total stress and pore pressure will be monitored during the tests. To do so, one first defines the Lagrangian porosity of a porous medium by the ratio of the pore volume V_ϕ to the initial total volume $V_0 (\phi = V_\phi / V_0)$. The volumetric strain is given by $\varepsilon_v = -d\,V / V_0$. Under changes in isotropic total stress σ (positive

in compression), the volumetric behaviour of a saturated sample depends on the changes in pore fluid pressure u and in differential stress $\sigma_d = \sigma - u$, also called Terzaghi effective stress.

2.1. Isotropic poroelasticity

The poroelastic expressions of the changes in total volume V and in pore volume V_ϕ with respect to changes in differential pressure σ_d and pore pressure u are defined by four compression modulus K_d, K_s, K_p, K_ϕ according to the following relations:

$$-\frac{dV}{V_0} = \frac{1}{K_d} d\sigma_d + \frac{1}{K_s} du \tag{1}$$

$$-\frac{dV_\phi}{V_{\phi_0}} = \frac{1}{K_p} d\sigma_d + \frac{1}{K_\phi} du \tag{2}$$

These moduli are defined by the following relations:

$$\frac{1}{K_d} = -\frac{1}{V_0}\left(\frac{\partial V}{\partial \sigma_d}\right)_u, \quad \frac{1}{K_p} = -\frac{1}{V_{\phi_0}}\left(\frac{\partial V_\phi}{\partial \sigma_d}\right)_u \tag{3}$$

$$\frac{1}{K_s} = -\frac{1}{V_0}\left(\frac{\partial V}{\partial u}\right)_{\sigma_d}, \quad \frac{1}{K_\phi} = -\frac{1}{V_{\phi_0}}\left(\frac{\partial V_\phi}{\partial u}\right)_{\sigma_d} \tag{4}$$

Note that these relations could also be written in terms of compressibility coefficients c_i with $c_i = 1/K_i$.

The drained bulk modulus K_d and the modulus K_p in equation (1) are obtained by running an isotropic drained compression test in which the confining stress is increased while keeping the pore pressure constant and while monitoring the changes in total volume V and pore volume V_ϕ, respectively.

The parameters of equation (2) are determined by running an unjacketed compression test, in which equal increments of confining stress and pore pressure are simultaneously applied to the sample, keeping constant the differential stress σ_d. The changes in sample volume with respect to changes in pressure provide the unjacketed modulus K_s. The changes in pore volume with respect to changes in pressure theoretically provide the unjacketed pore modulus K_ϕ. Note however that the experimental evaluation of this parameter is quite difficult, if not impossible, since the fluid volume exchanged during the test and monitored through the pressure volume controller is significantly affected by the fluid compressibility and the deformation of the both the pressure volume controller and the drainage system (Ghabezloo *et al*., 2008).

As quoted by Detournay and Cheng (1993), during an unjacketed test, a specimen of ideal porous material, homogeneous and isotropic at the micro-scale, would deform as if all pores were filled with the solid phase, resulting in a uniform volumetric strain for both the skeleton and the solid phase. In such a case, $K_\phi = K_s = K_m$, where K_m is the bulk modulus of the single solid constituent of the ideal porous material. This is why the unjacketed modulus K_s is also called the solid phase modulus in the literature. However, since the COx claystone is a micro-heterogeneous material in which the solid phase is composed of various minerals with distinct moduli, the expression of unjacketed modulus is preferred for K_s. In fact, the modulus K_s is some kind of weighted average of the bulk moduli of the constituents, the nature of which is not exactly known. However, Ghabezloo and Sulem (2009) evaluated the unjacketed modulus of the Rothbach sandstone using Hill's (1952) average formula and observed good accordance with the experimental data. The relation between the modulus K_ϕ and the material properties appeared to be quite complex and the K_ϕ value is generally not bounded by the elastic moduli of the solid components (Berryman, 1992). However, the assumption $K_s = K_\phi$ is generally adopted in the literature in numerical simulations.

As shown by Zimmerman *et al*. (1986), based on Betti's reciprocal theorem, the following relation holds between the elastic moduli K_p , K_d and K_s:

$$\frac{1}{K_p} = \frac{1}{\phi_0}\left(\frac{1}{K_d} - \frac{1}{K_s}\right) \tag{5}$$

Equation (1) can be rewritten in the following form to find the expression of Biot effective stress variation $d\sigma' = d\sigma - b du$:

$$d\varepsilon_v = -\frac{dV}{V_0} = \frac{1}{K_d}\left[d\sigma - du + \frac{K_d}{K_s} du \right] = \frac{1}{K_d}\left(d\sigma - b\, du\right) \tag{6}$$

Biot effective stress coefficient b is thus defined by:

$$b = 1 - \frac{K_d}{K_s} \tag{7}$$

Expression (6) shows that a test in which pore pressure is changed under constant total stress ($d\sigma = 0$) provides the following relation between the volume change and the pore pressure change:

$$d\varepsilon_v = -\frac{b}{K_s} du \tag{8}$$

Biot modulus H can thus be defined as follows:

$$\frac{1}{H} = \frac{1}{V_0}\left(\frac{\partial V}{\partial u}\right)_{\sigma} = \frac{b}{K_d} = \frac{1}{K_d} - \frac{1}{K_s} \tag{9}$$

Expression (9) shows that knowing the drained modulus K_d, the determination of H provides an indirect evaluation of both the Biot coefficient b and the unjacketed modulus K_s.

Using Eqs. (1), (2), (5) and (8) one can write the variation of the Lagrangian porosity $\left(d\phi/\phi_0 = dV_\phi/V_{\phi_0}\right)$ in the following form:

$$d\phi = -b\, d\varepsilon_v + \frac{1}{N} du \;;\; \frac{1}{N} = \frac{b}{K_s} - \frac{\phi_0}{K_\phi} \tag{10}$$

where N is the Biot's skeleton modulus that relates the changes in pore pressure and porosity when strains are held constant.

The undrained condition is defined as a condition in which the fluid mass is kept constant in the sample ($dm_w = 0$ where $m_w = \rho_w \phi$ is the fluid mass per unit volume of the porous sample). An undrained isotropic compression test is carried out in a triaxial/isotropic cell by closing the valves of the drainage system and by measuring the change in pore pressure u with respect to changes in isotropic compression stress σ. Two parameters can be determined, the undrained bulk modulus K_u and the Skempton coefficient B (Skempton, 1954), defined as follows:

$$B = \left(\frac{du}{d\sigma}\right)_{m_f}, \frac{1}{K_u} = -\frac{1}{V_0}\left(\frac{dV}{d\sigma}\right)_{m_f} \tag{11}$$

The changes in water mass dm_w in undrained conditions is null, resulting in the relation $\mathrm{d}m_w = \phi \mathrm{d}\rho_w + \rho_w \mathrm{d}\phi = 0$. The term $d\phi$ is given by equation (10) and the change in water unit mass is given by expression $d\rho_w/\rho_w = du/K_w$ (where K_w is the water modulus). Using these relations, one can find the following expression for the Skempton coefficient B (Skempton, 1954).

$$B = \frac{\left(\frac{1}{K_d} - \frac{1}{K_s}\right)}{\left(\frac{1}{K_d} - \frac{1}{K_s}\right) + \phi_0\left(\frac{1}{K_w} - \frac{1}{K_\phi}\right)} \tag{12}$$

By replacing $du = B\, d\sigma$ in equation (6) the following relation can be obtained for the undrained bulk modulus:

$$K_u = \frac{K_d}{1 - b\, B} \tag{13}$$

The experimental program followed here is based on the previous equations. It aims at characterizing the various poroelastic parameters by running different tests to examine the compatibility between the results obtained, in an aim to get satisfactory confidence in the experimental determination of the poroelastic parameters.

2.2. Transverse isotropic poroelasticity

The COx claystone is known as being transversely isotropic like many clayey sediments, with a preferential average orientation of the clay particles along a bedding plane that can be observed in scanning electron microscopy (e.g. Menaceur, 2014). The samples tested in this work have been cored perpendicular to the bedding planes. The anisotropic properties of the COx claystone have been detected in particular by Escoffier (2002), Chiarelli (2000), Andra (2005), Mohajerani *et al*., (2012), Zhang *et al*. (2012). Typically, the axial stiffness is larger than radial one. Zhang *et al*., (2012) performed a series of mini-compression tests on samples parallel and perpendicular to bedding planes under different relative humidities (RH). They observed a significant structural anisotropy reflected by a ratio of Young moduli E_2/E_1 (with E_2 and E_1 parallel and perpendicular to bedding, respectively) varying between 1.6 and 1.9 (increasing with decrease of RH). The Young moduli measured at RH = 98% of are $E_1 = 1.35$ GPa and $E_2 = 2.22$ GPa, respectively. Note that these values are smaller than the values currently used in numerical simulations with E taken equal to 4 GPa (Gens et *al*., 2007; Charlier *et al*., 2013). As a consequence, an anisotropic response can be expected from the isotropic compression paths planned in this work, as observed by Noiret *et al*. (2010) on the Tournemire shale.

Anisotropic poroelasticity has been considered by several authors, including Thompson and Willis (1991), Detournay and Cheng (1993), Cheng (1997) and Zimmerman (2000). The generalized Hooke's law for a porous material is given by the relation $\underline{\varepsilon} = \underline{\underline{C}}^{-1}\left(\underline{\sigma} - \underline{b}u\right)$ (Cheng, 1997) where $\underline{b}$ is the Biot's coefficient tensor and $\underline{\underline{C}}^{-1}$ the compliance tensor for a transverse isotropic material given by :

$$\underline{\underline{C}}^{-1} = \begin{pmatrix} \frac{1}{E_1} & \frac{-\nu_{12}}{E_1} & \frac{-\nu_{12}}{E_1} \\ \frac{-\nu_{12}}{E_1} & \frac{1}{E_2} & \frac{-\nu_{23}}{E_2} \\ \frac{-\nu_{12}}{E_1} & \frac{-\nu_{23}}{E_2} & \frac{1}{E_2} \end{pmatrix} \tag{14}$$

In the case of a transverse isotropic material submitted to an isotropic stress increment ($d\sigma_1 = d\sigma_2 = d\sigma_3 = d\sigma$) the stress-strain relation can be written in the following form:

$$d\varepsilon_1 = \frac{1}{E_1}\left(d\sigma - b_1\, du\right) - \frac{2\nu_{12}}{E_1}\left(d\sigma - b_2\, du\right) \tag{15}$$

$$d\varepsilon_2 = -\frac{\nu_{12}}{E_1}\left(d\sigma - b_1\, du\right) + \frac{\left(1-\nu_{23}\right)}{E_2}\left(d\sigma - b_2\, du\right) \tag{16}$$

in which the x_1 axis is taken perpendicular to bedding with x_2 and x_3 parallel to bedding. E_1 is the Young modulus along direction x_1 perpendicular to bedding and ν_{12} the Poisson ratio in the (x_1, x_2) plane. E_2 and ν_{23} are the Young modulus and the Poisson ratio in the (x_2, x_3) plane, respectively. For symmetry reasons, the Young moduli and Poisson ratios verify the relation $\nu_{12}/E_1 = \nu_{21}/E_2$.

After Cheng (1997), the Biot coefficients b_1 and b_2 are defined by equations (15) and (16)

$$b_1 = 1 - \frac{M_{11} + 2M_{12}}{3K_s} \tag{17}$$

$$b_2 = 1 - \frac{M_{12} + M_{22} + M_{23}}{3K_s} \tag{18}$$

where,

$$M_{11} = \frac{\mathrm{E}_1^2\left(1-\nu_{23}\right)}{\mathrm{E}_1 - \mathrm{E}_1\nu_{23} - 2\mathrm{E}_2\nu_{12}^2} \tag{19}$$

$$M_{12} = \frac{\mathrm{E}_2\ \mathrm{E}_1\nu_{12}}{\mathrm{E}_1 - \mathrm{E}_1\nu_{23} - 2\mathrm{E}_2\nu_{12}^2} \tag{20}$$

$$M_{22} = \frac{\mathrm{E}_2\left(\mathrm{E}_1 + \mathrm{E}_2\nu_{12}^2\right)}{\left(1+\nu_{23}\right)\left(\mathrm{E}_1 - \mathrm{E}_1\nu_{23} - 2\mathrm{E}_2\nu_{12}^2\right)} \tag{21}$$

$$M_{23} = \frac{\mathrm{E}_2\left(\mathrm{E}_1\nu_{23} + \mathrm{E}_2\nu_{12}^2\right)}{\left(1+\nu_{23}\right)\left(\mathrm{E}_1 - \mathrm{E}_1\nu_{23} - 2\mathrm{E}_2\nu_{12}^2\right)} \tag{22}$$

The combination of the different loading conditions considered here (drained, undrained, pore pressure changes and unjacketed conditions) allows writing the anisotropic modulus measured in each test from relations (15) and (16).

In the case of drained isotropic compression test where pore pressure is kept constant (du = 0), the measured anisotropic moduli, called D_1 and D_2 in directions x_1 and x_2, respectively, are given by the following relations :

$$\frac{1}{D_1} = \frac{d\varepsilon_1}{d\sigma} = \frac{1}{E_1}\left(1-2\nu_{12}\right) \tag{23}$$

$$\frac{1}{D_2} = \frac{d\varepsilon_2}{d\sigma} = -\frac{\nu_{12}}{E_1} + \frac{\left(1-\nu_{23}\right)}{E_2} \tag{24}$$

The measured anisotropic moduli in the case of the pore pressure test (change in pore pressure under constant confining pressure, $d\sigma = 0$) are called H_1 and H_2 in directions x_1 and x_2 and are given by the following relations:

$$\frac{1}{H_1} = \frac{d\varepsilon_1}{du} = -\frac{b_1}{E_1} + 2\nu_{12}\frac{b_2}{E_1} \tag{25}$$

$$\frac{1}{H_2} = \frac{d\varepsilon_2}{du} = \frac{\nu_{12}}{E_1} b_1 - \frac{(1-\nu_{23})}{E_2} b_2 \tag{26}$$

In the same way, one can write the anisotropic undrained moduli that can be measured when running an undrained isotropic compression test. During this test, the relation between the increments of pore pressure and total stress is $du = B\, d\sigma$, where B is the Skempton coefficient. The undrained anisotropic moduli U_1 and U_2 in directions x_1 and x_2 are given by:

$$\frac{1}{U_1} = \frac{d\varepsilon_1}{d\sigma} = \frac{1}{E_1}\left((1-b_1B) - 2\nu_{12}(1-b_2B)\right) \tag{27}$$

$$\frac{1}{U_2} = \frac{d\varepsilon_2}{d\sigma} = -\frac{\nu_{12}}{E_1}(1-b_1B) + \frac{(1-\nu_{23})}{E_2}(1-b_2B) \tag{28}$$

The unjacketed test (where $d\sigma = du$) can also provide the unjacketed anisotropic moduli S_1 and S_2 in directions x_1 and x_2, respectively, as follows:

$$\frac{1}{S_1} = \frac{d\varepsilon_1}{d\sigma} = \frac{1}{E_1}\left((1-b_1) - 2\nu_{12}(1-b_2)\right) \tag{29}$$

$$\frac{1}{S_2} = \frac{d\varepsilon_2}{d\sigma} = -\frac{\nu_{12}}{E_1}(1-b_1) + \frac{(1-\nu_{23})}{E_2}(1-b_2) \tag{30}$$

This poroelastic framework can now be used to interpret the data obtained with the high precision isotropic compression cell.

3. Material and methods

3.1. The Callovo-Oxfordian claystone

The mineralogical composition of the COx claystone and more specifically the clay and carbonate contents, vary with depth. The total porosity is estimated between 14% in carbonated levels and 19.5% in more argillaceous levels (Yven *et al*., 2007). At the level of the Bure URL, the COx claystone is made up of a clay matrix (45-50% clay fraction) in which are embedded 20-30% carbonates, 20-30% quartz and a small fraction of feldspar. The clay fraction is composed of 10-24% mixed layer illite/smectite, 17-21% illite, 3-5% kaolinite, 2-3% chlorite (Gaucher et *al*., 2004). The smectite fraction of the mixed layer illite/smectite is estimated between 50 and 70%. It provides to the COx claystone some swelling properties (e.g. Mohajerani *et al*., 2012; Delage *et*

al., 2014) and interesting self-sealing capabilities (Davy *et al*., 2007; Zhang, 2011; Menaceur *et al*., 2015b).

The specimens tested in this study (EST31912c and e) come from 80 mm diameter cores that were extracted at the depth of the Bure URL (490 m). Two specimens of 38 mm diameter and 10 mm height were cored by using a diamond core in the direction perpendicular to the bedding plane and cut at the required length by using a diamond saw. The water content was obtained by weighing the sample before and after oven drying at 105°C during 48 hours. The sample volume was determined by hydrostatic weighing to calculate the total connected porosity and the initial degree of saturation. The specimen EST31912c was tested immediately after coring. Its initial water content was equal to 7.45%, corresponding to a degree of saturation of 94.2%, considering a particle density of 2.70 g/cm^3 (Andra 2005). The specimen EST31912e, that was tested two months later, was preserved from evaporation by plunging it in a mix 70% paraffin 30% vaseline oil and wrapping it in plastic film. Its water content however decreased to 4.54% during the conservation period, corresponding to a degree of saturation of 67.8%. The initial characteristics of the two specimens tested are presented in Table 1. A suction measurement was carried out on some cuttings of specimen EST31912c by using a chilled mirror tensiometer (WP4, Decagon), providing a value of 19.7 MPa for a specimen with a degree of saturation of 94.2%. These data are representative of a good preservation of the specimen. They are in good compatibility with the water retention curves provided by Pham *et al*. (2007) and Wan *et al*. (2013). This measurement was unfortunately not carried out on specimen EST31912e.

3.2. Experimental device

The experimental device developed in this work is an extension of a system initially developed by Tang *et al*. (2008) to investigate the thermal behaviour of compacted bentonites. It was further developed by Mohajerani *et al*. (2012) to investigate thermal pressurization in the COx claystone. As shown in Figure 1, it is composed of a thermal isotropic compression cell connected to two pressure-volume controllers (PVC, GDS Brand) imposing pressures up to 60 MPa. Compared to previous works, the sample diameter was reduced to 38 mm in order to add a local system of axial and radial strains measurement by mean of LVDTs (Figure 1a). The short height of the sample (10 mm with drainage at bottom) results in a short drainage length that ensures a good saturation within a reasonable period of time and good drainage (see Monfared *et al*., 2011a). Drainage was ensured by a thin geotextile on specimen EST31912c. To reduce the compressibility of the drainage system, the geotextile was replaced by a porous disk for specimen EST31912e. The difference between the two drainage systems (geotextile and porous disk) slightly affects the

measurement of the undrained parameters. A correction of the parasite effects of the pore volume of the drainage system is presented in the Appendix. Monfared (2011) checked the drainage performances of the geotextile under pressure. To insulate the sample from the confining fluid (silicone oil), a specially designed cylindrical neoprene membrane able to continuously envelop the top and lateral face of the sample was used, without using any piston or porous disk on the top of the sample. The membrane was tightly fixed to the bottom base by means of two O-rings.

As shown in Figure 1-b, the cell was immersed in a temperature-controlled bath. Pore pressure changes in the sample were measured by a pressure transducer (0 to 75 MPa range) placed outside the bath to avoid any perturbation due to the temperature changes in the bath. The temperature of the bath was controlled with 0.1°C accuracy and measured by means of a thermocouple. One of the two ducts arriving at the sample bottom was connected to the pressure transducer whereas the other one was connected to the back pressure PVC. This PVC was carefully filled by demineralized and de-aired water.

3.3. Strain measurement

The main improvement with respect to the device of Mohajerani *et al*. (2012) concerns the monitoring of the axial and radial strain by means of LVDTs, as shown in Figure 2. Given the stiffness of the COx claystone, with a Young modulus of about 4000-5600 MPa (Andra 2005; Gens *et al*., 2007; Charlier *et al*., 2013) and because of the small size of the sample, the displacements during compression are expected to be small (around 2 μm by MPa). To avoid any disturbance due to the neoprene membrane, direct contact between the LVDT stem and the specimen was ensured by piercing the membrane with a hole smaller in diameter than the stem. Good fluid tightness was ensured by putting a drop of neoprene glue on the membrane around the stem. Using this technique, displacement measurements were improved with a minimum accuracy of 0.1 μm corresponding to a strain of 10^{-5}.

Figure 3 shows a comparison during an undrained compression test between the data of the radial LVDT in direct contact with the specimen through the membrane and that obtained by the axial one in contact with the membrane. Starting from an initial confining stress of 12 MPa with a back pressure of 4 MPa, the confining stress was increased with a loading rate of 20 kPa/min and maintained at 16.5 MPa during 13 hours. Afterwards, an unloading-reloading path up to a maximum pressure of 18.5 MPa was followed. Finally, the confining stress was decreased down to 12 MPa with a loading rate of 10 kPa/min. The comparison between the two measurements clearly shows that the LVDT in direct contact with the sample precisely follows all the loading and unloading phases, while the measurements made on the membrane do not detect the unloading

phases at the 18 and 26th hours. The loading sequence at 20h is also poorly monitored. This clearly shows the improvement provided by ensuring a direct contact of the LVDT stem with the specimen through the membrane.

3.4. Saturation phase

As demonstrated in swelling soils (e.g. Delage *et al*. (2007) and applied by Monfared *et al*. (2011a) on the Opalinus clay and Mohajerani *et al*. (2011) and Menaceur *et al*. (2015a, 2015b) on the COx claystone, it is mandatory to saturate swelling soils and clay rocks under stress conditions close to in-situ one to minimize possible swelling and damage. To do so, the ducts and the geotextile were kept dry during the sample setup to avoid any contact of the sample with water. Once the sample placed on the base with the membrane put around and the cell placed and filled with the confining fluid (oil), vacuum was applied through the valve located close to the pressure transducer (valve V2 in Figure 2) so as to evacuate any trapped air between the membrane and the sample. Then, the confining pressure was increased to 8 MPa, a value close to the in-situ Terzaghi effective stress. The drainage system under vacuum was afterwards filled with de-aired water through valve V2 while valve V1 was kept closed, ensuring good saturation of the drainage system. Finally, the confining stress and pore pressure were simultaneously increased up to 12 MPa and 4 MPa respectively at a rate of 100 kPa/min to reach stress conditions close to in-situ.

Figure 4a shows the water exchange (i.e. the ratio of injected water ΔV_w monitored by the PVC with respect to the initial sample volume V_0) together with the volumetric strains measured by the LVDTs in tests EST31912c. The sample exhibit a small swelling (0.05%, at the limit of the precision of the PVC) with axial swelling larger than radial swelling. The monitoring of water exchanges does not seem to be satisfactory during the first day, but a-good compatibility of the volume changes with water exchanges is observed after one day.

The response of the axial LVDT is not satisfactory for sample EST31912e (Figure 4b) and no volume change could be calculated from local strain measurement. The radial strain stabilizes after one and a half day, like in sample EST31912c, but at a value significantly larger, a possible effect of the smaller initial degree of saturation.

A possible reason of the significant difference in the swelling response is the difference in initial degree of saturation, with values of 94.2% and 67.8% for samples EST31912c and EST31912e, respectively. Similar observations were made by Menaceur (2014) when testing in the oedometer two samples of COx samples with degrees of saturations of 77% and 91% and by Ewy (2015) who found larger swelling in shales and claystones with lower partial saturation.

Indeed, loss of water (drying) in clayey rocks results in damage and micro-cracks that enhance swelling.

3.5. Loading rates

When performing a drained compression test, the pore pressure field should remain homogeneous with negligible changes in pore pressure (Gibson and Henkel, 1954). Homogeneity of the pore pressure field is also mandatory when performing an unjacketed test or an undrained compression test. In practice, pore pressure can only be controlled at the sample borders connected with the drainage system. This occurs at the bottom of the 10 mm high cylindrical specimen in the isotropic compression tests carried out here. In all cases, pore pressure homogeneity can be ensured if a sufficiently low stress rate is adopted. The loading rates depends on the sample permeability, drainage length, material's stiffness and of the nature of the test carried out. It is impossible to have a perfectly homogeneous pore pressure distribution, however a loading rate can be considered as satisfactory for a given loading path when the generated pore pressure heterogeneity inside the sample has a negligible influence on the measured strains and consequently on the evaluated poroelastic parameters.

A loading rate of 0.5 kPa/min was adopted for the drained compression test, like in Sultan *et al*. (2000) on the Boom clay and Monfared *et al*. (2011a) who used a hollow cylinder triaxial cell with 10 mm drainage length on Boom clay and Opalinus clay. This value was validated by poroelastic numerical simulations performed to investigate pore pressure homogeneity and the effect of the loading rate on the measurement of the moduli in all the tests performed, including that in which pore pressure was changed under constant total stress. A loading rate of 2 kPa/min appeared to be satisfactory for the unjacketed test.

3.6. Correction of drainage system effect for the undrained experiments

Undrained compression tests are run by increasing the confining pressure while all valves of the drainage system are closed. The confining pressure variation results in a simultaneous change of the sample pore pressure. The measurement of the pore pressure change by the pressure transducer inevitably requires some fluid mass exchange between the pore volumes of the sample and of the drainage system. The loading rate should thus be slow enough to ensure pore pressure equilibrium between these pore volumes. Therefore, the undrained condition ($\Delta m_w = 0$) cannot be ensured in the pore volume of the sample only, it is actually imposed in the larger volume including the pore volumes of both the specimen and the drainage and pore pressure measurement system. This artefact induces some error in the measured undrained parameters due to the compressibility

of the drainage system and of the fluid filling it. A correction method should thus be applied to the measured parameters.

Wissa (1969) and Bishop (1976) were the first who proposed a correction method for the effect of the drainage system on the results of an undrained compression test. It was then extended by Ghabezloo and Sulem (2009, 2010) to correct the pore pressure and volumetric strain in an undrained heating test. This correction method has been applied, with some additional terms to take into account the presence of geotextile in the drainage system, to the results of experiments performed on Opalinus clay (Monfared *et al*., 2011a) and COx claystone (Mohajerani *et al*., 2012). The correction method is presented in the Appendix along with a parametric study on the effects of various parameters.

4. Experimental program and results

Various cycles in isotropic stress have been carried out to determine independently the five following poroelastic parameters:

- The unjacketed modulus K_s, determined by running an unjacketed compression test in which pore pressure and confining pressure are simultaneously increased, keeping the Terzaghi effective stress constant.
- The drained bulk modulus K_d, determined by running a drained isotropic compression test in which the confining pressure is increased under constant pore pressure.
- The Biot modulus H, determined by running a "pore pressure" test in which pore pressure is changed under constant total stress.
- The undrained bulk modulus K_u, determined by running an undrained isotropic compression test.
- The Skempton coefficient $B = \Delta u/\Delta\sigma$ determined by measuring the increase in pore pressure Δu resulting from an undrained isotropic compression under an increment of total stress $\Delta\sigma$.

The experimental program was carried out under initial isotropic Terzaghi effective stresses of 10 MPa for test EST31912c and 8 MPa for test EST31912e.

4.1. Unjacketed compression test

As seen in Eq. 1, a direct method to estimate the unjacketed modulus K_s consists in performing an unjacketed compression test by simultaneously increasing the confining pressure and the pore pressure ($\Delta\sigma = \Delta u$), hence keeping the differential (Terzaghi effective) stress constant. For proper determination of K_s, a good precision in strain measurements is necessary.

Moreover, the very low permeability of the COx claystone makes unjacketed compression tests quite long because of the small loading rate necessary to ensure a homogeneous pore pressure field. The results of an unjacketed test carried out with the high precision device of Figure 1 on sample EST31912c at a loading rate of 2 kPa/mn are presented in Figure 5. The isotropic confining pressure was increased from 14 MPa to 16 MPa and the pore pressure from 4 MPa to 6 MPa, keeping a constant value of the Terzaghi stress of 10 MPa. The data are presented in terms of change in axial and radial strain with respect to isotropic confining pressure. At maximum confining pressure (16 MPa) a maximum axial strain of 0.012% that corresponds to a displacement value of 0.8 μm (indicating the good performance of the local strain measurement) is measured. A significantly anisotropic response is observed with radial strains (ε_2, parallel to bedding) significantly smaller than axial ones (ε_1, perpendicular to bedding) and a ratio $\varepsilon_2/\varepsilon_1$ equal to 5.7. The isotropic equivalent unjacketed modulus obtained is equal to 21.73 GPa, corresponding to a compressibility coefficient c_s ($1/Ks$) equal to 0.046 GPa^{-1}.

4.2. Undrained compression test

The undrained compression test is aimed at providing the undrained bulk modulus K_u and the Skempton B coefficient. Both parameters are related by equation (13) and were determined along an unloading/reloading path to make sure to keep staying in the elastic domain.

4.2.1. Skempton coefficient

Figure 6 presents the changes in pore pressure as a function of the confining pressure during an undrained test run on sample EST31912c by unloading the confining stress from 14 MPa down to 12.8 MPa. The response is quite linear and the slope provides a measured value of the Skempton coefficient $B^{meas} = 0.63$.

The correction (see Appendix) provides a corrected value $B^{corr} = 0.84$, with a difference compared to B^{meas} of about 25%, mostly due to the compressibility of water and to the large dead volume of the drainage system (geotextile). This corrected Skempton coefficient B^{corr} is equal to that found in the COx claystone by Mohajerani *et al*. (2013) in a hollow cylinder triaxial cell. These authors demonstrated that $B = 0.84$ indicated a good saturation of the specimen.

Unfortunately, a leak occurred during the test on sample EST31912e and no B value could be obtained.

4.2.2. Undrained bulk modulus (K_u)

The measurement of the undrained bulk modulus was achieved on both samples with axial and radial strains monitored. Only one unloading sequence from 13.9 down to 12.8 MPa was carried out in the test on sample EST31912c. Four cycles were performed between 12 MPa and 11 MPa in the test on sample EST31912e, as seen in Figure 7 showing the changes in radial, axial and volumetric strains with respect to the confining pressure for both tests.

Linear responses with clear anisotropy are again observed in axial and radial strains with an anisotropy ratio of 3.7 and 3.5 for tests EST31912c and EST31912e, respectively. This ratio is quite different compared to that observed in the unjacketed test. Load cycles provide a satisfactory reversible response in the test on sample EST31912e (Figure 7b). The maximum strain measured by the radial LVDTs is equal to 0.003% (10^{-5}, say a displacement of 0.52 μm), and that measured by axial LVDT is 0.011%, say a displacement of 1.09 μm), confirming the high precision performance of the monitoring of the local strains.

The measured undrained moduli are K_u^{mes} = 7090 MPa for test EST31912c and K_u^{mes} = 6480 MPa for test EST31912e and they correspond to corrected values K_u^{cor} = 12420 MPa and K_u^{cor} = 10930 MPa, respectively. The significantly lower measured values are due to the high ratio between the volume of the drainage system and the sample volume (V_L/V) (see Appendix). The lower value of the undrained bulk modulus in test EST31912e compared to that in test EST31912c is due to the lower applied Terzaghi effective stress. The relatively good correspondence between the two values provides a good confidence in the K_u values obtained.

4.3. Drained compression test

The drained compression test conducted to determine the drained bulk modulus K_d was carried out by keeping the pore pressure constant (du = 0) by connecting valve V1 (Figure 1-b) to the PVC controlling the pore pressure (u = 4 MPa). A loading rate of 0.5 kPa/min was adopted to ensure satisfactory drained conditions with the drainage length of 10 mm. Thanks to the accuracy of the strain measurements, small stress cycles of only 500 kPa were applied, a small enough range to stay within the elastic domain.

Three drained unloading-reloading cycles were performed, one on sample EST31912c (between 14 MPa and 13.5 MPa) and two on sample EST31912e (between 12 MPa and 11.6 MPa and between 12 MPa and 11.4 MPa). Like in previous tests, the response in axial and radial strain indicates some anisotropy (Figure 8) with smaller radial strains with ratios □1/□2 of 2.3 and 2.4 for samples EST31912c and EST31912e, respectively. The good repeatability observed in the two cycles carried out on sample EST31912e (Figure 8b) provides good confidence in the results. One

also observes the stress dependency of the drained compressibility, with higher modulus obtained under higher Terzaghi effective stress. The average drained bulk modulus values obtained are equal to 2985 MPa (σ_d = 14 MPa) and 2027 MPa (σ_d = 12 MPa) for tests EST31912c and EST31912e, respectively.

4.4. Pore pressure loading test

Equation (9) shows that the Biot modulus H can be determined by running a test in which pore pressure is changed under constant total stress. Equation (9) also shows the relation between H, b, K_d and K_s. This test should be carried out under a slow rate of pressure change (0.5 kPa/mn), like in a drained test, to ensure uniform pore pressure distribution within the sample. The pore pressure was first increased from 4 MPa up to 4.8 MPa and then decreased, resulting in an unloading-reloading cycle in Terzaghi effective stress. As previously, the pressure change was chosen small enough to remain in the elastic domain and avoid any potential damage of the sample. As seen in Figure 9, the response is linear and anisotropic with smaller radial strains and an anisotropy ratio $\varepsilon_1/\varepsilon_2$ of 1.8 and 1.5 for samples EST31912c and EST31912e, respectively.

Like in the drained test, one observes the stress dependency of the Biot modulus (H) with respect to Terzaghi effective stress, with average values of 3470 MPa and 2237 MPa under 10 MPa and 8 MPa, respectively.

5. Analysis of experimental results and discussion

5.1. Overall compatibility of the equivalent isotropic parameters

The compatibility of the set of equivalent isotropic poroelastic parameters determined from the various tests is now examined within the isotropic poroelastic framework presented in Section 2. This compatibility analysis is similar to that performed by Ghabezloo *et al*. (2008) on a set of poroelastic parameters of a hardened cement paste. The unjacketed modulus K_s directly evaluated from the unjacketed test (K_s = 21730 MPa, see Figure 5) can also be calculated indirectly from the values of the drained bulk modulus (K_d) and the Biot's modulus (H) using equation (9). As seen in Table 2, the indirectly evaluated K_s values for both samples are very close to that measured in the unjacketed test. As expected, the values of K_d and H are stress dependent but they finally provide comparable (not stress dependent) values of K_s. This analysis shows the compatibility of the results of drained, unjacketed and pore pressure loading tests.

The Biot effective stress coefficient b can be determined by using the various poroelastic relations presented below ((31)-*a* to *c*) by combining the results of two tests among the four tests performed (drained, undrained, unjacketed compression and pore pressure loading tests).

Expressions (31)-*d* and (31)-*e* use the results of all tests to evaluate *b*. Note however that equations (c) and (d) cannot be used for sample EST31912e since the Skempton coefficient could not be measured.

$$b = \begin{cases} \dfrac{K_d}{H} & (a) \\ 1 - \dfrac{K_d}{K_s} & (b) \\ \dfrac{1}{B}\left(1 - \dfrac{K_d}{K_u}\right) & (c) \\ \dfrac{K_u}{BK_u + H} & (d) \\ \dfrac{K_u(K_s - K_d)}{K_s(K_u - K_d) + H(K_s - K_d)} & (e) \end{cases} \tag{31}$$

The Biot effective stress coefficients *b* calculated using the various expressions (31) are given in Table 3. One can see a good compatibility between the values calculated that vary between 0.84 and 0.89 with an average value of 0.87 for sample EST31912c and between 0.90 and 0.91 with and average value of 0.91 for sample EST31912e. Again, good overall compatibility of the set of poroelastic parameters of the COx claystone determined from the distinct tests performed is observed, with a stress dependency of the *b* coefficient (0.87 under $\sigma = 12$ MPa and 0.91 under $\sigma = 12$ MPa). This analysis shows again the overall compatibility between all the experiments and provides confidence in the parameters determined. One can then calculate the Skempton coefficient for sample EST31912e, providing a value of 0.90 using relation (31)-*c*.

Based on the elastic parameters adopted by Gens *et al*. (2007) and Charlier *et al*. (2013) (Young modulus $E = 4$ GPa and Poisson ratio $\nu = 0.3$), an equivalent drained bulk modulus $K_d = 3.3$ GPa in the case of isotropy could be calculated. Using equation (7), an equivalent *b* value of 0.85 is calculated using this value of K_d and the measured value of the unjacketed modulus $K_s = 21.73$ GPa. In other words, the damage of a laboratory sample tend to over-estimate the *b* parameter. Knowing the value of K_s, a reasonable value of the *b* parameter could be obtained if the elastic parameters of the in-situ claystone are carefully determined.

5.2. Effects of anisotropy on the unjacketed modulus

Figure 5 showed a significant anisotropy in the response of the unjacketed test, with a ratio $\varepsilon_1/\varepsilon_2$ of 5.7 indicating a compressibility perpendicular to bedding significantly larger than that parallel to bedding. This ratio is actually the highest one observed in all the tests carried out in this work.

The relation between the unjacketed modulus and the compressibility of the solid phase is complex in the case of composite materials and natural rocks made up of various minerals. The unjacketed modulus is an overall response depending on the one hand on the response in compression of the elementary particles and on the other hand, on the way particles are organised together, i.e on the fabric (or texture). It has been shown that most minerals (including quartz and calcite) exhibit a significant anisotropy with a dependence of the elastic modulus with respect to the direction (Bass 1995). This is suspected to be also true for clays platelets (and more particularly for the smectite phase) with a significant effect of adsorbed water molecules that should increase the compressibility when they are mobilised, i.e. when compression is carried out perpendicular to the platelet. Note that an isotropic overall response in unjacketed test with comparable axial and radial strains can be observed (Coyner 1984), in sandstone for instance, when elementary grains (with anisotropic response) can be randomly oriented within the rock fabric, thanks to their rounded shape. This is obviously not the case of the fabric of the COx claystone where calcite, quartz and other detritic grains are embedded in a clay matrix (50%). In this case, the anisotropic response of the solid phase that is mobilised during an unjacketed test results from the combined response of the clay matrix and of the embedded grains. The response of the matrix itself results from both the anisotropic response of the elementary clay platelets (mixed layered illite-smectite) and their preferred orientation along the bedding plane.

5.3. Effect of anisotropy on the Biot effective stress coefficient(s)

As shown in Section 2.2, the Biot b scalar coefficient defined in isotropic poroelastic media adopts a tensorial nature in transverse isotropic media, defined by two parameters b_1 and b_2 (Equations (17) and (18)).

In equations (23) to (30), one can see that the anisotropic ratio between the modulus measured along directions x_1 and x_2 for each test become equal if $b_1 = b_2$. However, the strain measurements made here through different experiments evidence some anisotropy that should affect the scalar nature of the b coefficient.

From equations (23) to (26), the Biot coefficients b_1 and b_2 can be written as a function of the measured parameters D_1, D_2, H_1, H_2 and of the unknown parameter ν_{12}, as follows:

$$b_1 = -2\nu_{12}\left[\left(\frac{\nu_{12}}{H_1}+\frac{1}{H_2}\right)\Big/\left(\frac{\nu_{12}}{D_1}+\frac{1}{D_2}\right)\right]-\left(1-2\nu_{12}\right)\frac{D_1}{H_1} \tag{32}$$

$$b_2 = -\left[\left(\frac{\nu_{12}}{H_1}+\frac{1}{H_2}\right)\Big/\left(\frac{\nu_{12}}{D_1}+\frac{1}{D_2}\right)\right] \tag{33}$$

Table 4 summarizes the measured anisotropic moduli obtained from the drained compression and from the pore pressure test on samples EST31912c and EST31912e. The difference between the ratio D_2/D_1 and H_2/H_1 is also shown. Now, the estimation of b_1 and b_2 is only dependent of the unknown parameter ν_{12}. The calculated values of b_1 and b_2 when ν_{12} is varied between two values considered as reasonable boundaries (0.25 and 0.35) are presented in Table 5.

One can see that the calculated values of b_1 and b_2 for each experiment show a weak dependency with respect to the changes in ν_{12}. Actually, the parameter ν_{12} could be measured by a triaxial shearing test, not planned in the present experimental program carried out in an isotropic compression cell. Note however that Menaceur *et al*. (2015b) obtained a ν_{12} value of 0.30 on the Callovo-Oxfordian claystone whereas Homand *et al*. (2006) provided a value of 0.35.

Adopting a value of 0.3 for ν_{12} provides values of $b_1 = 0.845$ and $b_2 = 0.896$ under 10 MPa Terzaghi effective stress on specimen EST31912c and of $b_1 = 0.870$ and $b_2 = 0.976$ under 8 MPa on specimen EST31912e. b_i parameters are smaller under lower stress, but specimen EST31912e, with smaller degree of saturation, is probably more damaged, another reason of having a smaller b value (Aublivé-Conil 2003).

6. Conclusion

The values of the poroelastic parameters of the Callovo-Oxfordian claystone are still debated with published values of Biot coefficient comprised between 0.3 and 1.0, and an average value of 0.6 generally adopted in numerical simulations. To provide further information on parameters that are of great importance in the hydro-mechanical modelling in the close field around deep geological repository of radioactive waste, an experimental program was conducted in a specially designed isotropic compression cell. High precision strain measurements were made possible by getting rid of the parasite effects of the rubber membrane. To do so, direct contact through the membrane between the LVDTs stem and the specimen has been permitted, improving significantly the accuracy of the measurements of radial and axial strains. Great care was also devoted to the saturation procedure that was carried out under stress conditions close to in-situ, following previous works (Monfared *et al*., 2011a, 2011b, 2012; Mohajerani et al., 2013; Menaceur et al., 2015a, 2015b) on low permeability claystSones (Callovo-Oxfordian claystone and Opalinus clay) and the Boom clay. Satisfactory drainage conditions were also ensured by adopting a small drainage length (10 mm) and low enough stress rates during isotropic compression. The parasite effects of the drainage system on the measurement of undrained parameters have also been corrected.

Various poromechanical experiments have been performed: drained and undrained isotropic compression tests, unjacketed compression test and pore pressure loading test. The experimental results provided a direct determination of the equivalent isotropic poroelastic parameters of the COx claystone: drained bulk modulus K_d, undrained bulk modulus K_u, Skempton coefficient B, unjacketed modulus K_s and Biot modulus H. A compatibility analysis has also been performed in the framework of linear isotropic poroelasticity. A very good compatibility was found between the results of various experiments, showing their good quality, demonstrating the robustness of the method and giving confidence in the experimental data obtained. The data showed the stress dependency of parameters K_d, K_u and H that increased with increased effective stress. An indirect evaluation of the unjacketed modulus K_s showed that it was not stress dependent. For the tested specimens, cored at a depth of 490 m in the Underground Research Laboratory of Bure with around 50% clay fraction, the value of the equivalent isotropic Biot effective stress coefficient was found equal to 0.91 under a stress state close to that prevailing in-situ (mean total stress of 12 MPa and pore pressure of 4 MPa).

The COx claystone exhibited a well-marked transverse isotropic response under isotropic compression with axial strains smaller radial ones. An analysis in the framework of transverse isotropic poroelasticity provided the relations between the Biot effective stress coefficients b_1 and b_2 and the Poisson's ratio ν_{12} and the various moduli measured in the experiments. A parametric study showed that b_1 and b_2 had a very low sensitivity with respect to changes in ν_{12}, allowing a reasonable estimation of b_1 and b_2 under the in-situ stress state with b_2 (parallel to bedding) equal to 0.976, slightly higher than b_1 (perpendicular to bedding), equal to 0.870. This difference is related to the mobilisation of the layers of water molecules adsorbed along the smectite faces in the mixed layer illite-smectite platelet within the clay matrix that results in a smaller stiffness perpendicular to bedding.

This work should be completed in the laboratory by poromechanical experiments under deviatoric loading to evaluate all the poroelastic parameters in the case of transverse isotropy. The variability and stress dependency of these parameters should also be studied.

The poroelastic parameters determined here are that of a laboratory specimen previously extracted from the rock mass and probably affected by coring, stress release, desaturation, evaporation, trimming and resaturation under in-situ stresses. Given the susceptibility of claystones to damage, it is probable that these successive effects have some consequences on the parameters determined, like for instance an over-estimation of the b Biot parameter. In this regard,

further investigation on the in-situ determination of the hydro-mechanical parameters of the claystone and the comparison of in-situ data with laboratory data remain necessary.

Appendix:

Correction of the effect of the drainage system in undrained tests

The expression of the corrected Skempton coefficient (B^{cor}) with respect to the measured one (B^{mes}) is given below (Monfared *et al*., 2011a). For the sake of simplicity the equations are written in terms of compressibility $c_i = 1/K_i$.

$$B^{corr} = \frac{B^{meas}}{1+\frac{1}{V\left(c_d+c_s\right)}\left(V_p c_{dp}+V_g c_{dg}-B^{meas}\left(V_p\left(c_{dp}+\phi c_w\right)+V_g c_{dg}+V_L\left(c_w+c_L\right)\right)\right)} \quad (34)$$

The corrected undrained compressibility (c_u^{cor}) is then written as:

$$c_u^{corr} = \frac{c_d - c_u^{meas}}{1+\frac{1}{V\left(c_d+c_s\right)}\left(V_p c_{dp}+V_g c_{dg}-\left(V_p\left(c_{dp}+\phi_p c_w\right)+V_g c_{dg}+V_L\left(c_w+c_L\right)\right)\frac{c_d-c_u^{meas}}{c_d-c_s}\right)} \quad (35)$$

where V_p, V_g and V_L are the volumes of the porous disk, geotextile and connecting lines, respectively and c_{dp}, c_{dg} and c_L their drained compressibilities. ϕ and ϕ_p are the porosities of the sample and the porous disk respectively. V, c_d, c_u, and B are the volume, the drained compressibility, the undrained compressibility and the Skempton coefficient of the sample. c_s is the unjacketed compressibility.

The volume of samples EST31912c and EST31912e are V=11795 mm^3 and V=13847 mm^3, respectively. The volume of the connecting lines, porous disk and geotextile are V_L=2412 mm^3, V_p=2268 mm^3 *and* V_g=113 mm^3, respectively. Monfared *et al*. (2011a) performed a calibration test on a dummy metal sample and found a drained compressibility of the connecting lines c_L=0.32 GPa^{-1}, a drained compressibility of the porous disk c_{dp}=1.02 GPa^{-1}, and a drained compressibility of the geotextile c_{dg}=9.33 GPa^{-1}. The porosity of the porous disk was ϕ_p=0.22. The water compressibility at 25°C is c_w=0.447 GPa^{-1} (Spang, 2002). The corrected undrained bulk modulus and Skempton coefficient presented in 4.2 are evaluated using these parameters.

A-1- Parametric study on the induced errors

A parametric study is presented here to better clarify the influence of various material and drainage system properties on the induced errors on different undrained parameters. The error on a quantity Q is evaluated as $(Q_{measured}-Q_{corrected})/Q_{corrected}$. The most influent parameters on the error

are the drained compressibility c_d, the porosity ϕ and the volume ratio of the drainage system to the volume of the tested sample V_L/V. In this study, we take three values of the drained compressibility c_d more or less equivalent to the ones of the COx claystone (0.1 GPa^{-1}, 0.3 GPa^{-1} and 0.6 GPa^{-1}) and $c_s = c_\phi = 0.05$ GPa^{-1}. The volume ratio V_L/V is taken equal to 0.21 which corresponds to our experiment, and to further analyse the effect of the dead volume, a second ratio of 0.05 is also taken. The porosity is varied from 0.03 to 0.45.

Figure 10 shows the error on the measurement of the Skempton coefficient. When the rock is relatively highly compressible ($c_d = 0.5$ GPa^{-1} and $c_d = 0.3$ GPa^{-1}), the range of error does not vary a lot between small and high porosities. A greater volume of the drainage system understimates the Skempton coefficient (B). The measured Skempton coefficient juggles between a slight underestimating and a slight overestimating when a geotextile is used. But with a lower compressibility, the error varies a lot as a function of the porosity. In fact, we can observe that for a volume ratio of 0.21 the Skempton coefficient is underestimated with an error of 44% in case of geotextile, for 0.03 porosity and it is overestimated with an error of 35% for 0.45 porosity. When a porous disk is used, the Skempton coefficient is always underestimated (from 65% to 22%) for the same volume ratio. The error is more important and B is highly overestimated if the volume ratio is smaller on the use of geotextile and a high porosity material.

The error made on the measurement of the undrained bulk modulus (K_u) is shown on Figure 11. Unlike for the Skempton coefficient, the error is more important for higher compressibilities. The effect of the volume ratio is more significant in the error on the measurement of K_u, as a large difference is shown between the two volume ratios. Once more, the error induced by the use of a porous disk is slightly more important than the geotextile.

References

Andra (2005) Synthesis argile: evaluation of the feasibility of a geological repository in argillaceous formation. < http://www.andra.fr/download/site-principal/document/ editions/266.pdf >.

Aublivé-Conil N (2003) Modélisation du comportement mécanique des argiles raides avec prise en compte de l'endommagement : application aux argilites de l'Est. PhD thesis, Université de Cergy Pontoise.

Bass JD (1995) Elasticity of Minerals, Glasses, and Melts. In: Thomas JA (ed) Mineral physics and crystallography: a handbook of physical constants. American Geophysical Union, pp 45–63

Bemer E, Longuemare P, Vincké O (2004) Poroelastic parameters of Meuse/Haute Marne argillites: effect of loading and saturation states. Appl Clay Sci 26:359–366.

Berryman JG (1992) Effective stress for transport propreties of inhomogeneous porous rock.pdf. J Geophys Res 17409–17429.

Bishop AW (1976) The influence of system compressibility on the observed pore-pressure response to an undrained change in stress in saturated rock. Géotechnique 26:371–375.

Charlier R, Collin F, Pardoen B, Talandier J, Radu JP, Gerard P (2013) An unsaturated hydro-mechanical modelling of two in-situ experiments in Callovo-Oxfordian argillite. Eng Geol 165:46–63.

Cheng AH (1997) Material coefficients of anisotropic poroelasticity. Int J Rock Mech Min Sci 34:199–205.

Chiarelli AS (2000) Étude expérimentale et modélisation du comportement mécanique de l'argilite de l'est. PhD thesis, Université Lille I.

Chiarelli AS, Shao JF, Hoteit N (2003) Modeling of elastoplastic damage behavior of a claystone. Int J Plast 19:23–45.

Coyner KB (1984) Effects of stress, pore pressure, and pore fluids on bulk strain, velocity, and permeability in rocks. PhD thesis, MIT.

Davy C a., Skoczylas F, Barnichon J-D, Lebon P (2007) Permeability of macro-cracked argillite under confinement: Gas and water testing. Phys Chem Earth, Parts A/B/C 32:667–680.

Delage P, Le T-T, Tang A-M, Cui YJ, Li XL (2007) Suction effects in deep Boom clay block samples. Géotechnique 57:239–44.

Delage P, Menaceur H, Tang A-M, Talandier J (2014) Suction effects in deep Callovo-Oxfordian claystone Suction effects in deep Callovo-Oxfordian claystone. Géotechnique Lett 4:267–271.

Detournay E, Cheng AH (1993) Fundamentals of Poroelasticity. Chapter 5 Compr Rock Eng Princ Pract Proj Vol II, Anal Des Method, ed C Fairhurst, Pergamon Press II:113–171.

Escoffier S (2002) Caractérisation expérimentale du comportement hydromécanique des argilites de Meuse Haute-Marne. PhD thesis, Institut National Polytechnique de Lorraine.

Ewy RT (2015) Shale/claystone response to air and liquid exposure, and implications for handling, sampling and testing. Int J Rock Mech Min Sci 80:388–401.

Gaucher E, Robelin C, Matray JM, Négrel G, Gros Y, Heitz JF, Vinsot A, Rebours H, Cassagnabère A, Bouchet A (2004) ANDRA underground research laboratory: Interpretation of the mineralogical and geochemical data acquired in the Callovian-Oxfordian formation by investigative drilling. Phys Chem Earth 29:55–77.

Gens A, Vaunat J, Garitte B, Wileveau Y (2007) In situ behaviour of a stiff layered clay subject to thermal loading : observations and interpretation. Géotechnique 207–228.

Ghabezloo S, Sulem J (2010) Effect of the volume of the drainage system on the measurement of undrained thermo-poro-elastic parameters. Int J Rock Mech Min Sci 47:60–68.

Ghabezloo S, Sulem J (2009) Stress dependent thermal pressurization of a fluid-saturated rock. Rock Mech Rock Eng 42:1–24.

Ghabezloo S, Sulem J, Guédon S, Martineau F, Saint-Marc J (2008) Poromechanical behaviour of hardened cement paste under isotropic loading. Cem Concr Res 38:1424–1437.

Gibson RE, Henkel DJ (1954) Influence of Duration of tests at Constant Rate of Strain on Measured "Drained" Strength. Géotechnique 4:6–15.

Hill R (1952) The Elastic Behaviour of a Crystalline Aggregate.pdf. Proc Phys Soc 65:349–354.

Homand F, Shao JF, Giraud A, Auvray C, Hoxha D (2006) Pétrofabrique et propriétés mécaniques des argilites. Comptes rendus Géoscience 338:882–891.

Hoxha D, Giraud A, Homand F, Auvray C (2007) Saturated and unsaturated behaviour modelling of Meuse-Haute/Marne argillite. Int J Plast 23:733–766.

Hu DW, Zhang F, Shao JF (2013) Experimental study of poromechanical behavior of saturated claystone under triaxial compression. Acta Geotech 31–36.

Menaceur H (2014) Comportement thermo-hydro-mécanique et microstructure de l'argilite du Callovo-Oxfordien. PhD thesis, Université Paris Est.

Menaceur H, Delage P, Tang A-M, Conil N (2015a) On the Thermo-Hydro-Mechanical Behaviour of a Sheared Callovo-Oxfordian Claystone Sample with Respect to the EDZ Behaviour. Rock Mech Rock Eng 6–8.

Menaceur H, Delage P, Tang A-M, Conil N (2015b) The thermo-mechanical behaviour of the Callovo-Oxfordian claystone. Int J Rock Mech Min Sci 78:290–303.

Mohajerani M, Delage P, Sulem J, Monfared M, Tang A-M, Gatmiri B (2012) A laboratory investigation of thermally induced pore pressures in the Callovo-Oxfordian claystone. Int J Rock Mech Min Sci 52:112–121.

Mohajerani M, Delage P, Sulem J, Monfared M, Tang A-M, Gatmiri B (2013) The Thermal Volume Changes of the Callovo–Oxfordian Claystone. Rock Mech Rock Eng 47:131–142.

Monfared M (2011) Couplages température-endommagement-perméabilité dans les sols et roches argileux. PhD thesis, Université Paris-Est.

Monfared M, Delage P, Sulem J, Mohajerani M, Tang A-M, De Laure E (2011a) A new hollow cylinder triaxial cell to study the behavior of geo-materials with low permeability. Int J Rock Mech Min Sci 48:637–649.

Monfared M, Sulem J, Delage P, Mohajerani M (2011b) A Laboratory Investigation on Thermal Properties of the Opalinus Claystone. Rock Mech Rock Eng 44:735–747.

Noiret A, Giot R, Bemer E, Giraud A, Homand F(2010) Hydromechanical behavior of Tournemire argillites : Measurement of the poroelastic parameters and estimation of the intrinsic permeability by œdometric tests.

Pham QT, Vales F, Malinsky L, Nguyen M-D, Gharbi H (2007) Effects of desaturation–resaturation on mudstone. Phys Chem Earth, Parts A/B/C 32:646–655.

Skempton AW (1954) The pore-pressure coefficients A and B. Géotechnique 4:143–147.

Sultan N, Delage P, Cui YJ (2000) Comportement thermomécanique de l'argile de Boom. Comptes Rendus l'Académie des Sci - Ser IIB - Mech 328:457–463.

Tang A-M, Cui Y-J, Barnel N (2008) Thermo-mechanical behaviour of a compacted swelling clay. Geotechnique 58:45–54.

Thompson M, Willis JR (1991) A Reformulation of the Equations of Anisotropic Poroelasticity. J Appl Mech 58:612–616.

Valès F, Nguyen Minh D, Gharbi H, Rejeb A (2004) Experimental study of the influence of the degree of saturation on physical and mechanical properties in Tournemire shale (France). Appl Clay Sci 26:197–207.

Vincké O, Longuemare P, Boutéca M, Deflandre J-P (1998) Ivestigation of the poromechanical behavior of shales in the elastic domain. Pap SPE 47589 1–6.

Wan M, Delage P, Tang A-M, Talandier J (2013) Water retention properties of the Callovo-Oxfordian claystone. Int J Rock Mech Min Sci 64:96–104.

Wileveau Y, Cornet FH, Desroches J, Blumling P (2007) Complete in situ stress determination in an argillite sedimentary formation. Phys Chem Earth 32:866–878.

Wissa AEZ (1969) Pore pressure measurement in saturated stiff soils. J Soil Mech Found Div Am Soc Civ Eng 95 (SM4):1063–1073.

Yven B, Sammartino S, Geraud Y, Homand F, Villieras F (2007) Mineralogy, texture and porosity of Callovo-Oxfordian argilites of the Meuse/Haute-Marne region (eastern Paris Basin). Mémoires la société Géologique Fr 0249-7546:73–90.

Zhang CL (2011) Experimental evidence for self-sealing of fractures in claystone. Phys Chem Earth 36:1972–1980.

Zhang CL, Rothfuchs T (2004) Experimental study of the hydro-mechanical behaviour of the Callovo-Oxfordian argillite. Appl Clay Sci 26:325–336.

Zhang F, Xie SY, Hu DW, Gatmiri B (2012) Effect of water content and structural anisotropy on mechanical property of claystone. Appl Clay Sci 69:79–86.

Zimmerman RW (2000) Coupling in poroelasticity and thermoelasticity. 37:79–87.

Zimmerman RW, Somerton WH, King MS (1986) Compressibility of porous rocks. J Geophys Res 91:12765–12777.

Figure captions

Figure 1. (a) Isotropic compression cell; (b) Overall system with controlled temperature bath

Figure 2. Displacement measurement system

Figure 3. Accuracy of strain measurement in contact with the rock

Figure 4. Saturation phase: (a) sample EST31912c, (b) sample EST31912e

Figure 5. Unjacketed test (EST31912-c), pressure-strain response in loading phase

Figure 6. Skempton coefficient measured for test EST31912c

Figure 7. Undrained isotropic compression tests: (a) EST31912c, (b) EST31912e

Figure 8. Drained isotropic compression cycles: (a) EST31912c, (b) EST31912e

Figure 9. Pore pressure loading-unloading test: (a) EST31912c, (b) EST31912e

Figure 10. Parametric study of the error on Skempton coefficient (B)

Figure 11. Parametric study of the error on the undrained modulus (K_u)

Table captions

Table 1. Initial characteristics of the studied specimens

Table 2. Calculated K_s from measured K_d and H.

Table 3. Calculation of the Biot effective stress coefficient b.

Table 4. Measured anisotropic modulus in drained and pore pressure tests.

Table 5. Calculation of b_1 and b_2 for different ν_{12}.

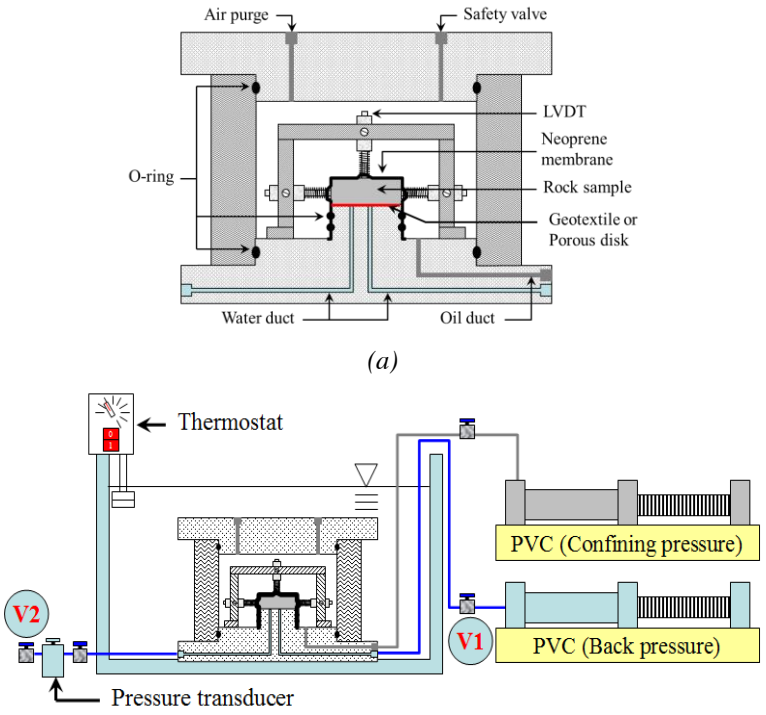

Figure 1. (a) Isotropic compression cell; (b) Overall system with controlled temperature bath

Figure 2 Click here to download Figure Figure (2).docx

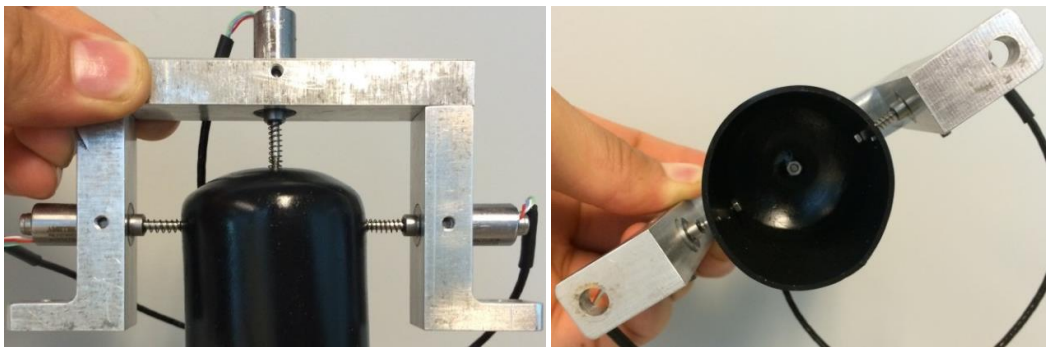

Figure 2. Displacement measurement system

Click here to download Figure Figure (3).docx

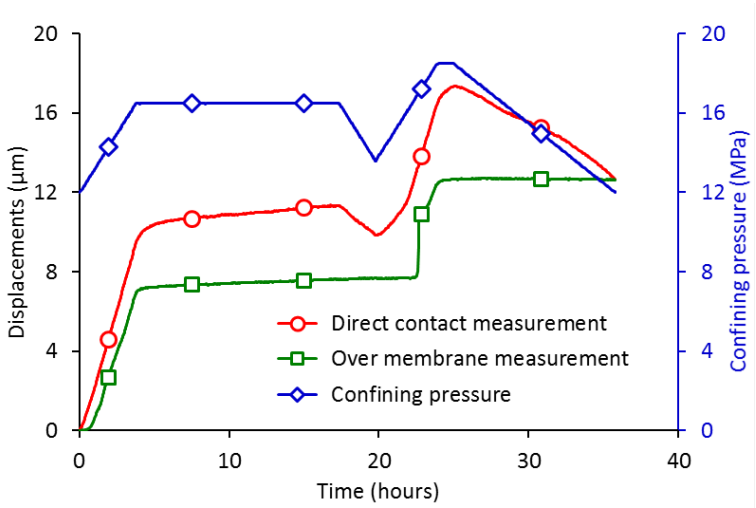

Figure 3. Accuracy of strain measurement in contact with the rock.

Click here to download Figure Figure (4).docx

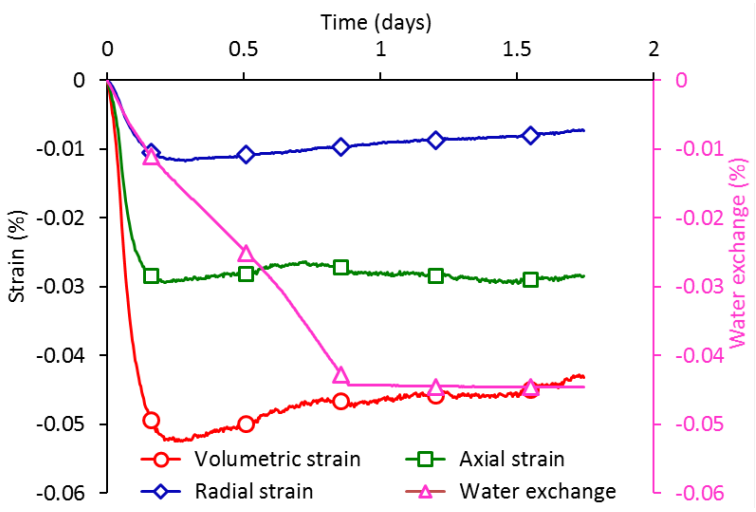

(a)

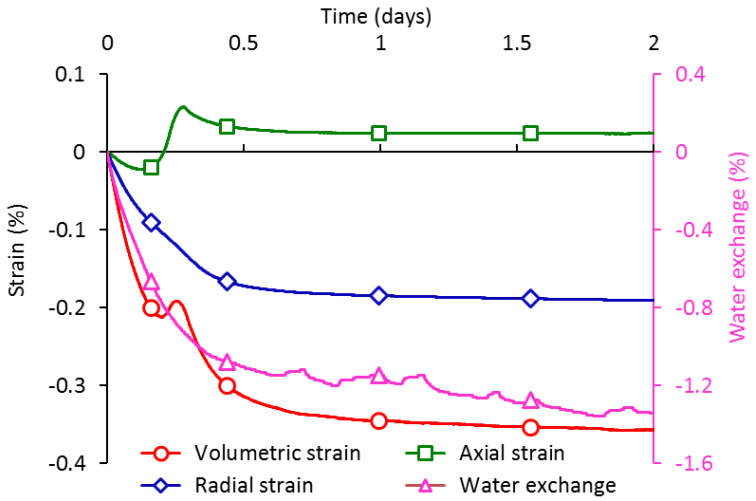

(b)

Figure 4. Saturation phase: (a) sample EST31912c, (b) sample EST31912e.

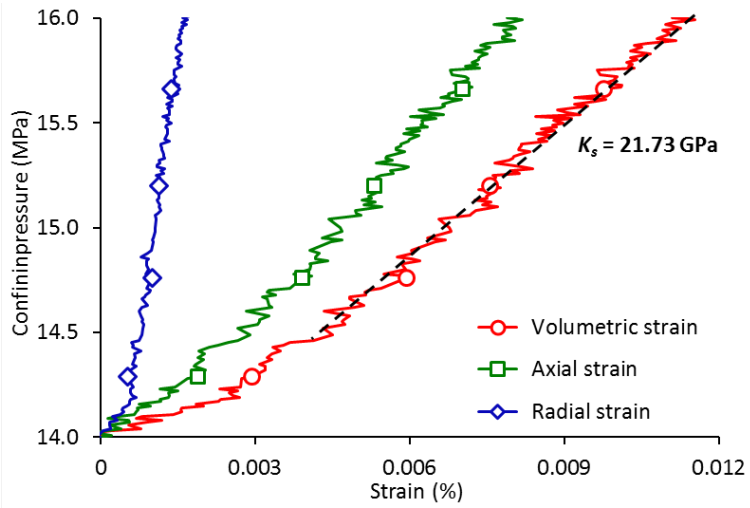

Figure 5. Unjacketed test (EST31912-c), pressure-strain response in loading phase

Click here to download Figure Figure (6).docx

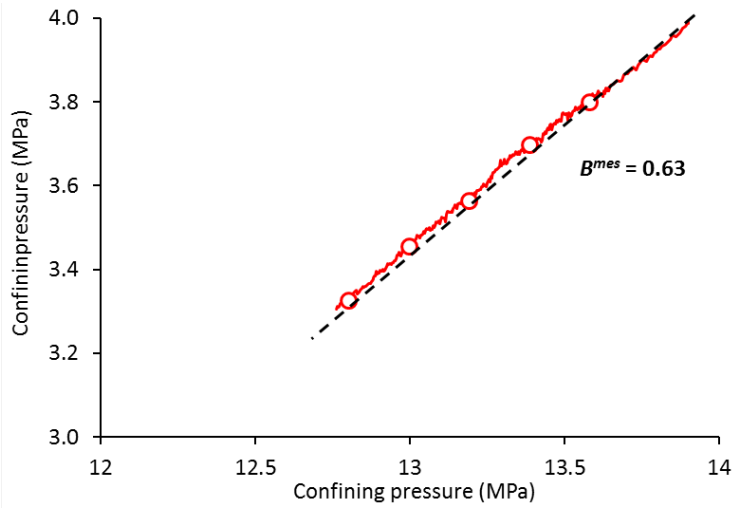

Figure 6. Skempton coefficient measured for test EST31912c

Click here to download Figure Figure (7).docx

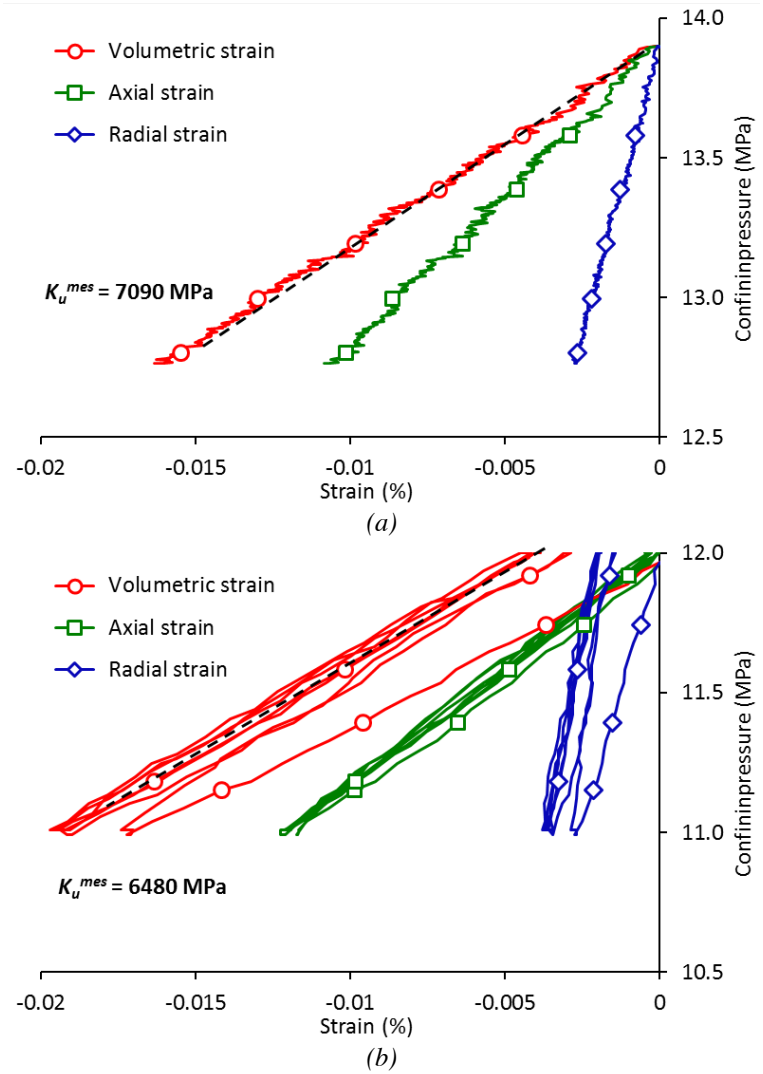

Figure 7. Undrained isotropic compression tests: (a) EST31912c, (b) EST31912e.

Click here to download Figure Figure (8).docx

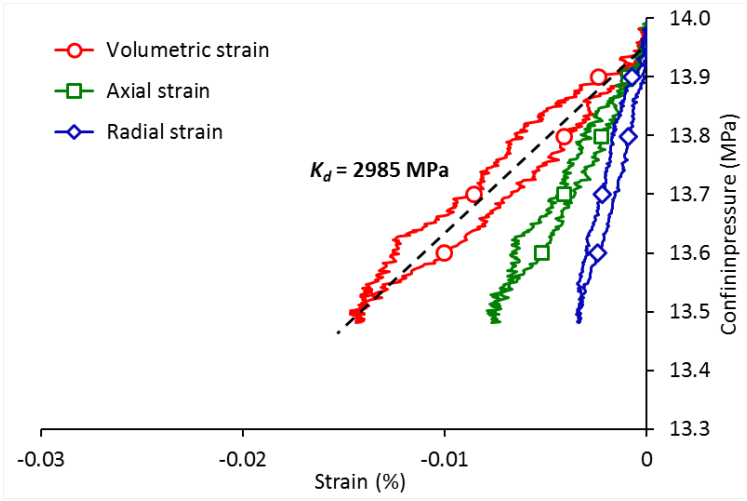

(a)

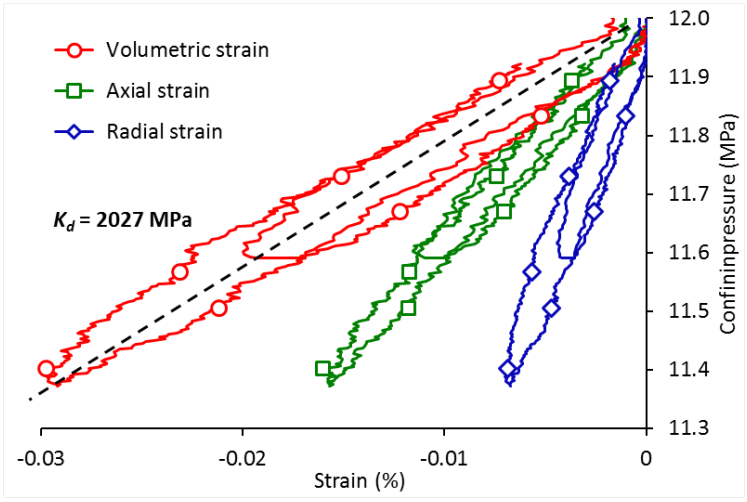

(b)

Figure 8. Drained isotropic compression cycles: (a) EST31912c, (b) EST31912e.

Click here to download Figure Figure (9).docx

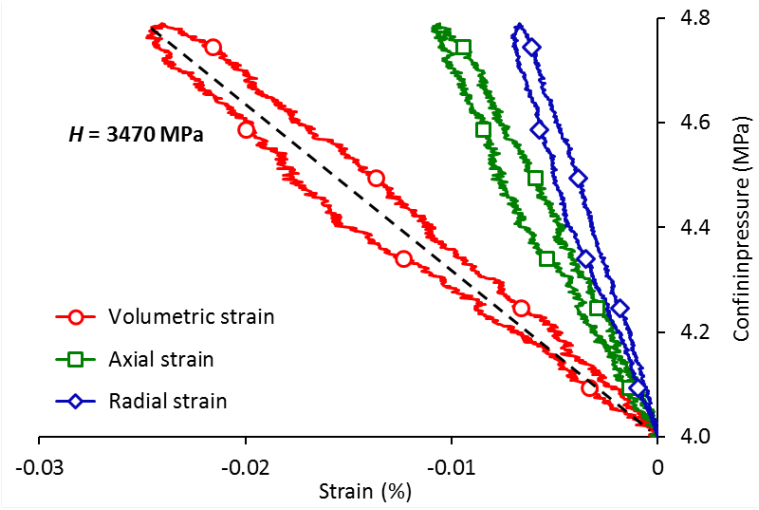

(a)

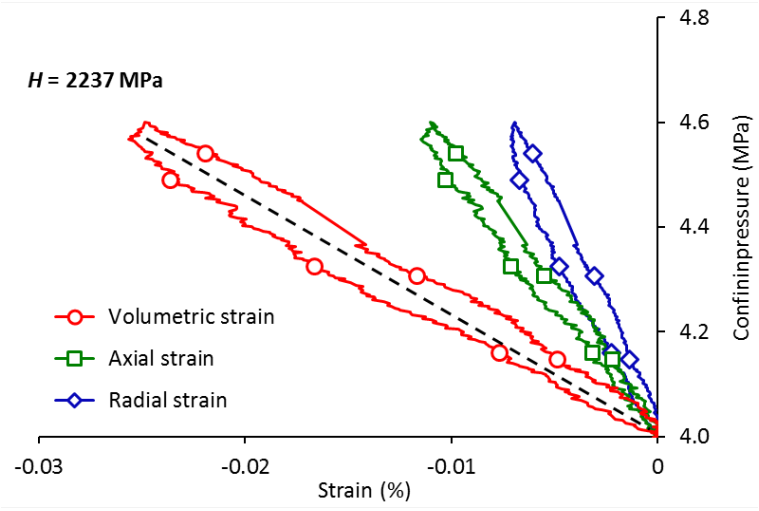

(b)

Figure 9. Pore pressure loading-unloading test: (a) EST31912c, (b) EST31912e.

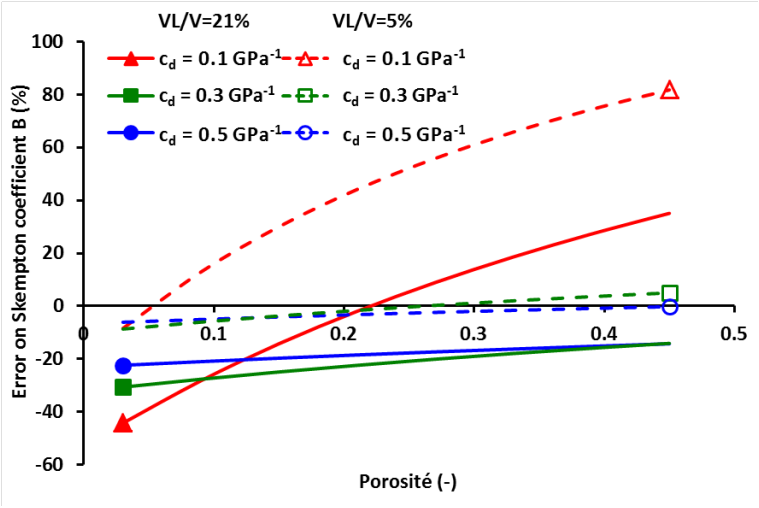

(a) Geotextile

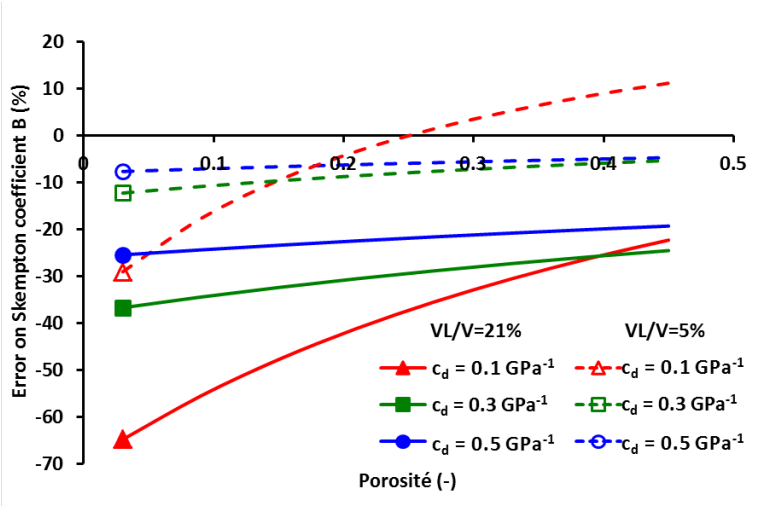

(b) Porous disk

Figure 10. Parametric study of the error on Skempton coefficient (B)

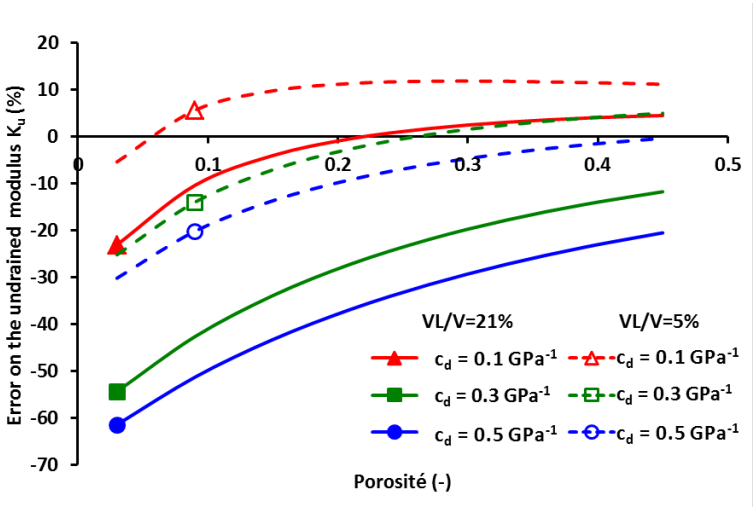

(a) Geotextile

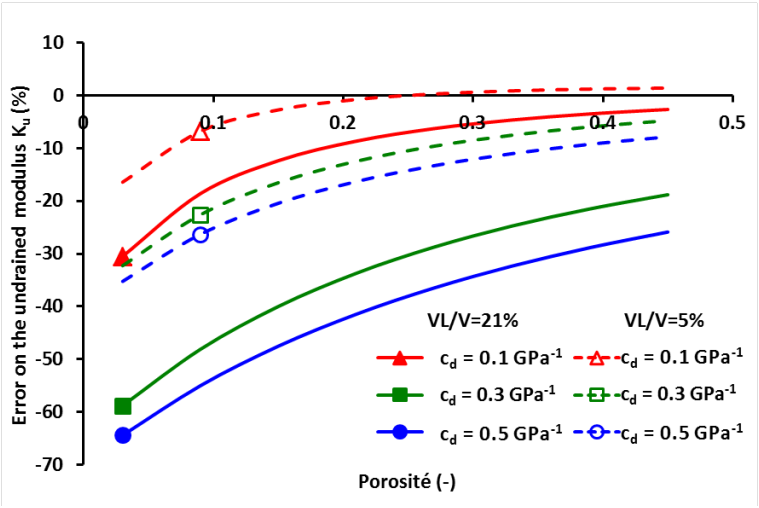

(b) Porous disk

Figure 11. Parametric study of the error on the undrained modulus (K_u)

Click here to download Table Table (1).docx

Table 1. Initial characteristics of the studied specimens

ID Ech.	w (%)	ρ (g/cm^3)	ρ_d (g/cm^3)	e	S_r (%)	ϕ (%)	Suction (MPa)
EST31912c	7.45	2.39	2.22	0.21	94.2	17.6	19.7
EST31912e	4.54	2.39	2.29	0.18	67.8	15.3	-

Table 2. Calculated K_s from measured K_d and H.

	EST31912c (σ_d = 10 MPa)	EST31912e (σ_d = 8 MPa)
Measured K_d (Figure 8)	2985 MPa	2027 MPa
Measured H (Figure 9)	3470 MPa	2237 MPa
Calculated K_s	21357 MPa	21592 MPa
Measured K_s (Figure 5)	21730 MPa	

Table 3. Calculation of the Biot effective stress coefficient b.

		EST31912c (σ_d = 10 MPa)	EST31912e (σ_d = 8 MPa)
Unjacketed modulus K_s		21730 MPa	
Drained modulus K_d		2985 MPa	2027 MPa
Biot modulus H		3470 MPa	2237 MPa
Undrained modulus K_u		12424 MPa	10931 MPa
Skempton coefficient B		0.84	-
Biot's coefficient b	(a)	0.86	0.91
	(b)	0.85	0.90
	(c)	0.91	-
	(d)	0.89	-
	(e)	0.86	0.91
Mean Biot coefficient b		0.87	0.91

Table 4. Measured anisotropic modulus in drained and pore pressure tests.

	EST31912c ($\sigma_d = 10MPa$)	EST31912e ($\sigma_d = 10MPa$)
D_1 (GPa)	5.6	3.7
D_2 (GPa)	12.8	9
H_1 (GPa)	-7.3	-5.2
H_2 (GPa)	-13	-7.7
D_2/D_1	2.3	2.4
H_2/H_1	1.8	1.5

Click here to download Table Table (5).docx

Table 5. Calculation of b_1 and b_2 for different ν_{12}.

	EST31912c (σ_d = 10 MPa)		EST31912e (σ_d = 8 MPa)	
ν_{12}	b_1	b_2	b_1	b_2
0.25	0.836	0.906	0.854	0.996
0.3	0.845	0.896	0.870	0.976
0.35	0.852	0.888	0.884	0.959